Flux Balance Analysis of Photoautotrophic Metabolism

Avantika A. Shastri and John A. Morgan*

School of Chemical Engineering, Purdue University, 480 Stadium Mall Dr., West Lafayette, Indiana 47907

Photosynthesis is the principal process responsible for fixation of inorganic carbon dioxide into organic molecules with sunlight as the energy source. Potentially, many chemicals could be inexpensively produced by photosynthetic organisms. Mathematical modeling of photoautotrophic metabolism is therefore important to evaluate maximum theoretical product yields and to deeply understand the interactions between biochemical energy, carbon fixation, and assimilation pathways. Flux balance analysis based on linear programming is applied to photoautotrophic metabolism. The stoichiometric network of a model photosynthetic prokaryote, *Synechocystis* sp. PCC 6803, has been reconstructed from genomic data and biochemical literature and coupled with a model of the photophosphorylation processes. Flux map topologies for the hetero-, auto-, and mixotrophic modes of metabolism under conditions of optimal growth were determined and compared. The roles of important metabolic reactions such as the glyoxylate shunt and the transhydrogenase reaction were analyzed. We also theoretically evaluated the effect of gene deletions or additions on biomass yield and metabolic flux distributions.

Introduction

Photoautotrophic metabolism is an amazingly complex process that utilizes widely available solar energy to incorporate inorganic carbon dioxide into the organic molecules required for life. Photosynthetic organisms include plants, algae, and some classes of bacteria. The incorporated carbon ends up in highly diverse molecules, from dietary elements such as carbohydrates, proteins, and vitamins, specialty compounds such as pigments, flavors, and fragrances, to extremely valuable pharmaceuticals (Figure 1). The field of metabolic engineering focuses on the manipulation of metabolic systems to efficiently produce valuable products (*1*). These efforts encompass expression of foreign enzymes and pathways in host organisms as well as the directed creation of mutant strains. Such manipulations naturally have a direct impact on the metabolic flux distributions in the system.

System-wide metabolic flux characterization is recognized as an important part of metabolic engineering not only in microbial systems but also in plants (*2*). One approach toward a quantitative understanding of the interactions between light and central metabolism is through kinetic modeling (*3*, *4* and references therein). These models are typically used to focus on small sections of metabolism, since the number of kinetic parameters that need to be determined increases with the complexity of the model. An alternative approach that requires a minimal amount of experimental data is stoichiometric modeling of biochemical reaction networks. This type of modeling is based on steady state mass balances on metabolic intermediates within a cell, requiring only the stoichiometric coefficients of biochemical reactions and maximum uptake and excretion rates of nutrients and products (*5*). Stoichiometric modeling therefore enables the modeling of a system-wide metabolic network. The model thus generated can be used to predict yields and generate flux maps under different environmental conditions and genetic backgrounds.

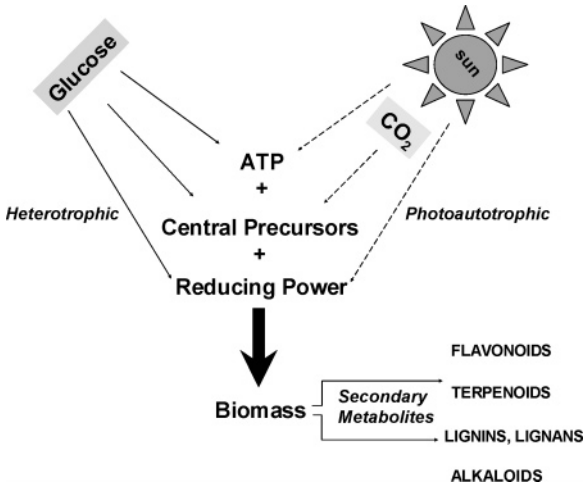

Figure 1. Fundamental differences between heterotrophic and autotrophic metabolism. In contrast to heterotrophs, autotrophs have independent sources of carbon and energy. Autotrophic metabolism in plants leads to the production of a wide variety of structurally and functionally diverse classes of valuable natural products.

Stoichiometric models of metabolism are typically underdetermined systems of linear algebraic equations. A popular approach to solve the equations is to use linear programming (*6*). The system of equations is solved for the unknown fluxes by formulating an objective function (like maximization of product or minimization of energy utilization) and searching the solution space for an optimum flux distribution that meets the objective. Varma and Palsson were the first to model the metabolic network of an entire organism (*Escherichia coli*) by the application of linear programming to stoichiometric

* To whom correspondence should be addressed. Tel: 1-765-494-4088. Fax: 1-765-494-0805. Email: jamorgan@purdue.edu.

10.1021/bp050246d CCC: $30.25
Published on Web 11/01/2005

modeling (*6*). Subsequently, the metabolism of several model microbes such as *Haemophilus influenzae* (*7*), *Helicobacter pylori* (*8*), *Aspergilus niger* (*9*), *Saccharomyces cerevisiae* (*10*), and *Chlorella pyrenoidosa* (*11*) has been studied using stoichiometric models. The flux balance approach has also been used to predict gene knockouts and heterologous gene additions in *E. coli* that lead to improved yields of succinate, lactate, and 1,3-propanediol and increased production of certain amino acids, respectively (*12*).

Photoautotrophic organisms have several unique aspects of metabolism different from microorganisms previously analyzed. Unlike heterotrophs, they possess distinct sources of carbon and energy inputs for growth (Figure 1). Thus, the interactions between the carbon substrate and energetic states of the system are expected to be different from those in heterotrophic systems.

The major contribution of this work is to extend the linear programming based flux balance approach to photoautotrophic metabolism, using *Synechocystis* sp. PCC 6803 as a model system. *Synechocystis* sp. PCC 6803 is a unicellular cyanobacterium that can grow photoautotrophically on carbon dioxide and light, as well as heterotrophically on glucose. It has a fully sequenced genome (*13*, *14*), thereby making it amenable to reconstruct a stoichiometric model. These features make it a popular model photosynthetic organism studied by many researchers. In this study, we reconstructed the stoichiometric biochemical network of the central metabolism of *Synechocystis* sp. PCC 6803 and evaluated its metabolic capabilities under photoautotrophic, mixotrophic, and heterotrophic conditions using flux balance analysis. We discuss several important aspects of the modeling, including the choice of a suitable basis for autotrophic growth and the handling of independent inputs of light and carbon dioxide to the system. A significant output of this modeling effort is stoichiometrically balanced fluxes that are invaluable as initial estimates for the experimental determination of autotrophic metabolic fluxes. We also examine several rationally selected metabolic engineering targets and their effects on the flux maps and biomass yields.

Materials and Methods

Metabolic Network Reconstruction. A stoichiometric network of biochemical reactions was reconstructed from the *Synechocystis* genomic database (*14*) and other biochemical literature. Although a keyword search in the *Synechocystis* database for the glyoxylate shunt enzymes (isocitrate lyase and malate synthase) did not result in any hits, the glyoxylate shunt was included in the network on the basis of evidence obtained by ^{13}C-labeled glucose feeding experiments (*15*). Obviously, the Calvin cycle enzymes responsible for carbon fixation form a key structure of the network. An important feature of the model is that *Synechocystis* has a discontinuous TCA cycle due to lack of α-ketoglutarate dehydrogenase (αkg dehydrogenase), which catalyzes the conversion of α-ketoglutarate into succinyl CoA. We have included a membrane-bound transhydrogenase reaction that converts $NADP^+$ and NADH to NADPH and NAD^+, respectively, coupled with the simultaneous translocation of two protons into the cytosol (*16*). Two important anapleurotic enzymes, PEP carboxylase and an NAD^+-dependent malic enzyme, are also included in the model. *Synechocystis* is not known to secrete fermentation byproducts such as ethanol, acetate, or succinate (*17*). We experimentally analyzed the extracellular broth of photoautotrophically grown *Synechocystis* using HPLC with a refractive index detector and could not detect any fermentation products (data not shown). Hence these reactions were not included in the model. We did not model reactions leading to storage products (such as glycogen or PHB) explicitly.

Photophosphorylation. Conversion of light energy into ATP (photophosphorylation) and the generation of NADPH (reducing power) by water oxidation were modeled through the cyclic and noncyclic electron transport processes (*18*, *19*). The cyclic electron transport chain (ETC) consists of several membrane-bound and membrane-associated electron carriers that are centered on a light-harvesting complex called photosystem I (PSI). The energy of electrons excited by light harvested by PSI and associated pigments is used to generate a proton motive force (PMF) via the pumping of H^+ across a membrane. This is coupled to a membrane-bound ATPase that utilizes these protons to generate ATP. Stoichiometrically, this process can be lumped into a single equation:

$$1 \text{ absorbed photon} \rightarrow 2\ H^+_{\text{external}} \quad (1)$$

The noncyclic electron transport chain generates both ATP and NADPH required for biosynthesis. It involves two light-harvesting complexes, photosystem I (PSI) and photosystem II (PSII). Electrons required for reducing $NADP^+$ to NADPH are derived from splitting of water in the PSII complex. Two photons are required to excite two electrons in the PSII complex. These electrons are then carried by several intermediate electron transporters to PSI. Two more photons excite two electrons in PSI, which are transferred to $NADP^+$ via ferredoxin. This process also generates a PMF that leads to ATP production. For every two electrons transported down the electron transport chain, a net of four H^+ are transported across the membrane and an additional two H^+ derived from H_2O also contribute toward the PMF. Additionally, the reduction of one NADPH requires two electrons. Thus, we model noncyclic electron transport as

$$4 \text{ photons} + NADP^+ + H_2O \rightarrow NADPH + 6\ H^+_{\text{external}} + 0.5\ O_2 \quad (2)$$

It has recently been shown that chloroplast ATPases require 14 H^+ molecules per three ATPs produced (*17*). Thus, the ATPase stoichiometric reaction was modeled as

$$4.67\ H^+_{\text{external}} + ADP \rightarrow ATP \quad (3)$$

Although the two modes of electron transport share several common electron carriers (e.g., ferredoxin, quinone pool, cytochrome b_6f complex, PSI, etc.), some researchers hypothesize that the cyclic and noncyclic electron transport systems in chloroplasts do not interfere with each other because of spatial separation in the thylakoid membranes (*20*). We have therefore modeled cyclic and noncyclic electron transport chains as independent, noninteracting events.

The fraction of incident solar radiation that is usable by photosynthetic systems resides in the 400−700 nm range and is called photosynthetically active radiation (PAR). The amount of PAR incident per unit area is called photosynthetic photon flux density (PPFD) and is expressed as moles of incident PAR photons per area per second. The photons in the stoichiometric model correspond to photons absorbed in the PAR range. Further, the light flux values in this work are based on the fraction

of the incident PPFD that is actually converted into chemical energy by the system, as described by eqs 1 and 2. The efficiencies of light-harvesting mechanisms and photochemical energy transduction also determine the fraction of the incident PPFD that is actually converted into chemical energy. These efficiencies are characterized using quantum yields of the photosystems (*21*). Factors such as vessel geometry and stirring efficiency further affect the percent of incident light absorbed. Thus, typically only a small percentage of the incident light flux is actually converted into usable chemical energy and reducing power. These phenomena have not explicitly been included in our model.

Autotrophic Growth Conditions. A 1-L culture of *Synechocystis* was cultivated autotrophically in a 1.25-L bioreactor (Bioflo 3000, New Brunswick Scientific, NJ) under a surface light flux of 150 μE/m^2/s in BG-11 medium (American Type Culture Collection medium 616) buffered with 10 mM HEPES under atmospheric levels of carbon dioxide at 30 °C. The pH was controlled at 7.5 $\pm$ 0.1. Growth was monitored spectrophotometrically by measuring the optical absorbance of cultures at 600 and 730 nm.

Maximum Uptake Rates. To perform simulations of growth, it is necessary to add constraints for maximum nutrient and light uptake rates. The maximum growth rate of photoautotrophically cultivated *Synechocystis* was measured to be 0.085 $\pm$ 0.015 h^{-1} from four separate experiments. This value is consistent with other reported values (*22*). The carbon balance (in the absence of overflow products) and the growth rate were then used to calculate the maximum CO_2 uptake rate as 3.70 mmol CO_2/g biomass/h. The maximum glucose uptake rate under heterotrophic conditions was found to be 0.85 mmol glucose/g biomass/h (*23*). An extreme upper bound of 2100 μE/m^2/s was set on the basis of the maximum available solar light flux (*24*). These parameters are used as additional constraints in the model.

Cell Surface Area Estimation. An estimation of total cellular surface area per kilogram of biomass was made as follows. The mass of a typical *Synechocystis* cell was taken to be 0.5 pg (*25*). The diameter of the *Synechocystis* cell was assumed to be 1.75 μm (*26*) with a spherical geometry. The surface area/kg biomass is therefore calculated to be 19245 m^2. This value enables the conversion of light flux calculated per kilogram of biomass into units of μE/m^2/s.

Maintenance Requirements. Maintenance requirements are frequently determined experimentally in terms of maintenance coefficients and maintenance yields (*27*), which are inconvenient to directly apply to stoichiometric models. For *E. coli*, Palsson and co-workers addressed this issue by expressing maintenance requirements as a certain number of ATP per glucose molecule consumed (*28*). By a similar procedure, the experimental (*23*) and simulated biomass yields were matched. We determined the maintenance requirement for the heterotrophic case to be 1.67 ATP per glucose consumed, which is equivalent to 18.61 ATP per kilogram of biomass formed. The maintenance requirements for the autotrophic and mixotrophic cases were also assumed to be the same.

Linear Programming Problem Formulation. A steady-state material balance was written on all involved metabolites (intracellular, substrates, and products) to obtain the governing set of linear algebraic equations (*4*). A reaction was classified as reversible if the enzyme responsible is known to catalyze both the forward and backward reaction in vivo. Reversible reactions were decomposed into two separate reactions, and each flux was constrained to be nonnegative, as is required for convexity of the flux space. The system consisted of 28 irreversible and 42 reversible reactions, forming a total of 70 unknown fluxes (v_i) of central carbon metabolism. Mass balances were written on 46 intracellular metabolites. Binary variables y_i were introduced such that

$$v_i = 0 \Rightarrow y_i = 0 \tag{4}$$

$$v_i \neq 0 \Rightarrow y_i = 1 \tag{5}$$

Fluxes were constrained to allow only one direction of the reversible reaction to be active (see eq 10).

The final model was formulated as follows: max (or min) objective function subject to

$$\sum_j s_{ij} v_j = 0 \text{ for every } i \in M_\mathrm{i} \tag{6}$$

$$\sum_j s_{ij} v_j \leq 0 \text{ for every } i \in M_\mathrm{r} \tag{7}$$

$$\sum_j s_{ij} v_j \geq 0 \text{ for every } i \in M_\mathrm{p} \tag{8}$$

$$v_j \geq 0 \tag{9}$$

$$y_i + y_{i+1} \leq 1 \tag{10}$$

where s_{ij} is the stoichiometric coefficient of the ith metabolite in the jth reaction, v_j is the flux of the jth reaction, M_i is the set of internal metabolites, M_r is the set of reactants other than the substrate, and M_p is the set of products excreted (including O_2 and CO_2 when applicable). The matrix $\mathbf{S} = \{s_{ij}\}$ represents the reaction network structure. Seventy enzymes involved in intermediary metabolism (amino acid biosynthetic pathways) were also included in the model in the form of the biomass formation equation from central precursors. The corresponding reactions are listed in Supporting Information. Maximum uptake rates of glucose and CO_2 were added as constraints. For the auto- and mixotrophic growth modes, the CO_2 input fluxes were defined as additional constraints.

A mixed integer linear program was formulated in the GAMS environment (GAMS Development Corporation, Washington, DC) and the optimum solution was found using the ILOG CPLEX 8.100 solver (ILOG, inc. Mountain View, CA).

Selection of Basis. Carbon and energy in form of ATP and NAD(P)H are two of the main components required for growth. In contrast to heterotrophic organisms where sugars such as glucose both provide the carbon skeletons and prompt the release of NADH and ATP by catabolism, photoautotrophic metabolism has distinct sources of carbon mass and energy (Figure 1). The selection of a basis for photoautotrophic metabolism could therefore be based on either carbon or light limitation. A simulation maximizing biomass flux, based on an input of a net CO_2 uptake per time per unit biomass, leads to a certain optimal biomass flux v_b (kg biomass formed/time/kg dry weight). In the case of photoautotrophic growth, CO_2 is the only carbon input into the system. Also, in *Synechocystis*, the absence of overflow products implies that biomass is the only carbon output; v_b is therefore tantamount to the carbon balance. A comparison of biomass yields (kg biomass/C input) under different network configurations (e.g., upon deletion or addition of an enzyme) is therefore of little utility, since they lead to

Table 1. Precursor Demand and Byproducts for Biomass Formation in *Synechocystis*[a]

	stoichiometric coefficient				stoichiometric coefficient				stoichiometric coefficient		
metabolite	A	H	M	metabolite	A	H	M	metabolite	A	H	M
ATP	−53.35	−39.21	−38.89	PYR	−1.197	−2.64	−2.44	ADP	53.35	39.21	38.89
R5P	−0.715	−0.399	−0.382	OAA	−2.039	−1.23	−1.14	$NADP^+$	49.06	27.22	29.01
AcCoA	−3.727	−4.64	−3.96	αKG	−1.233	−1.04	−0.886	FUM	0.683		
G6P	−1.191	−0.882	−1.228	SUCCoA	−0.16			Ac	0.103		
E4P	−0.501	−0.406	−0.376	NADPH	−49.06	−27.22	−29.01	SUC	0.16		
NAD^+	−2.82	−2.82	−2.82	GAP	−0.133	−0.238	−0.208	biomass	1	1	1
3PG	−1.205			CO_2	1.017	1.834	1.834	NADH	2.82	2.82	2.82
PEP	−1.002	−1.53	−1.42	CoA	3.887	4.64	3.96				

[a] A = autotrophic, H = heterotrophic, M = mixotrophic cases. The negative sign indicates consumption, positive sign indicates formation. All quantities are in moles, except biomass (kg).

the same yield value. Therefore, the pertinent question to address in the photoautotrophic system is to find an optimal flux distribution that maximizes biomass formation while utilizing the least amount of (light) energy. Consequently, a meaningful comparison becomes the amount of energy required to produce a unit of biomass.

Two-Step Optimization Strategy. For the autotrophic case, we used a two-step optimization strategy, where our first objective is to maximize biomass with a net input of a 100 mol of CO_2/h. The light flux to the system is a free flux (constrained to a maximum solar PPFD). The obtained biomass flux is added as a constraint to the next optimization step, and the optimal flux distribution is determined with minimization of light energy utilization.

Biomass Composition. The protein concentration from mid-exponential phase photoautotrophic cultures was measured spectrophotometrically using a Pierce BCA protein assay kit standard (Pierce Biotechnology, IL). The amino acid composition was estimated from GC−MS data of hydrolyzed protein (data not shown). Carbohydrate percentage was analyzed spectrophotometrically at 490 nm by the phenol−sulfuric acid method (*29*) and lipids were measured by chloroform−methanol extraction (*30*). The percentage of nucleic acids was calculated as the balance, adding up to a 100%. The elemental composition of dry biomass was also determined.

Results and Discussion

Biomass Synthesis Equation. The protein-to-carbohydrate ratio in mid-exponential growth phase was measured to be 2.60 ± 0.1 g protein (BSA)/g carbohydrates (glucose), from three replicates. The lipid fraction was found to be 9 ± 4% of the dry weight from two independent measurements. The elemental composition of biomass was found to constitute 51.38% C, 6.8% H, 11.29% N, 27.51% O, and 3.3% others. The nucleic acids were divided into 17% RNA and 3% DNA constituents (*31*). The final composition of mid-exponential photoautotrophically growing *Synechocystis* was found to be 51% proteins, 19% carbohydrates, 10% lipids, and 20% nucleic acids. The final carbon and nitrogen balances were within 1.8% and 6.5% of the elemental analysis. To account for the reduction of nitrate into ammonia, 4 mol of NADPH was added per mole of nitrate. On the basis of the above composition, biomass formation from central metabolic precursors was formulated into an equation as shown in Table 1. This equation is based on a kilogram of biomass, and the stoichiometric coefficients of all other metabolites represent molar quantities. The equation was included in the stoichiometric model to represent a lumped flux toward biomass formation. For the heterotrophic and mixotrophic cases, biomass formation equations formulated by Yang et al. (*23*) were used (Table 1).

Metabolic Flux Topologies under Different Environments. *Synechocystis* is known to possess three fundamentally different modes of metabolism. These are photoautotrophic growth, where net carbon dioxide is fixed in the presence of light as the energy source, heterotrophic growth utilizing glucose and deriving energy from respiration, and mixotrophic growth, where the organism simultaneously utilizes CO_2, light energy, and glucose for growth. Analysis of the photoautotrophic growth condition is important since it represents the primary biological process that leads to the synthesis of organic molecules from free sunlight and CO_2. The heterotrophic growth on glucose simulates night-time metabolism, where the organism breaks down stored carbon (such as glycogen) into glucose and derives energy to meet its metabolic needs in the absence of light energy. Potentially, mixotrophic metabolism provides a way to obtain improved growth yields in industrial photobioreactors. The heterotrophic and autotrophic modes of operation clearly represent the two extreme limits of mixotrophic metabolism.

We simulated autotrophic growth on CO_2 and light using the two-step optimization process (see Methods). As expected, the flux map obtained on a basis of 100 mol of CO_2 by minimizing energy utilization (Figure 2) reveals that the autotrophic flux flows in the gluconeogenic direction and through the reductive mode of the pentose phosphate pathway (Calvin cycle). PEP carboxylase serves as an anapleurotic enzyme to the TCA cycle. The photosynthetic quotient (moles of O_2 released per mole of CO_2 fixed) was found to be 1.46, which falls within the observed range for several photosynthetic organisms (*32*).

Heterotrophic growth on glucose was simulated by maximizing growth in the absence of light (Figure 3). In contrast to the autotrophic case, the glycolytic and the oxidative pentose phosphate pathways were found to be active. The topology of the TCA cycle included flux through the glyoxylate shunt, succinate dehydrogenase, and the malic enzyme. The transhydrogenase reaction did not participate in the optimum flux distribution.

In the case of mixotrophic metabolism, there exist three independent inputs of glucose, CO_2 and light to the system. To handle these parameters, the simulations were performed in the following manner. Using heterotrophic metabolism as the base case, the system was provided a maximum glucose uptake rate of 0.85 mol/kg biomass/h and the CO_2 uptake flux was left unconstrained. A series of optimizations were performed by progressively providing greater amounts of light flux to determine the optimal flux distribution for maximization of biomass yield. Figure 4 shows the flux map for a case of mixotrophic metabolism where a photon flux of 0.184 $\mu E/m^2/s$ is provided in addition to 0.85 mol/kg cells/h glucose uptake. The topology clearly lies between the heterotrophic and autotrophic flux maps, with the reduc-

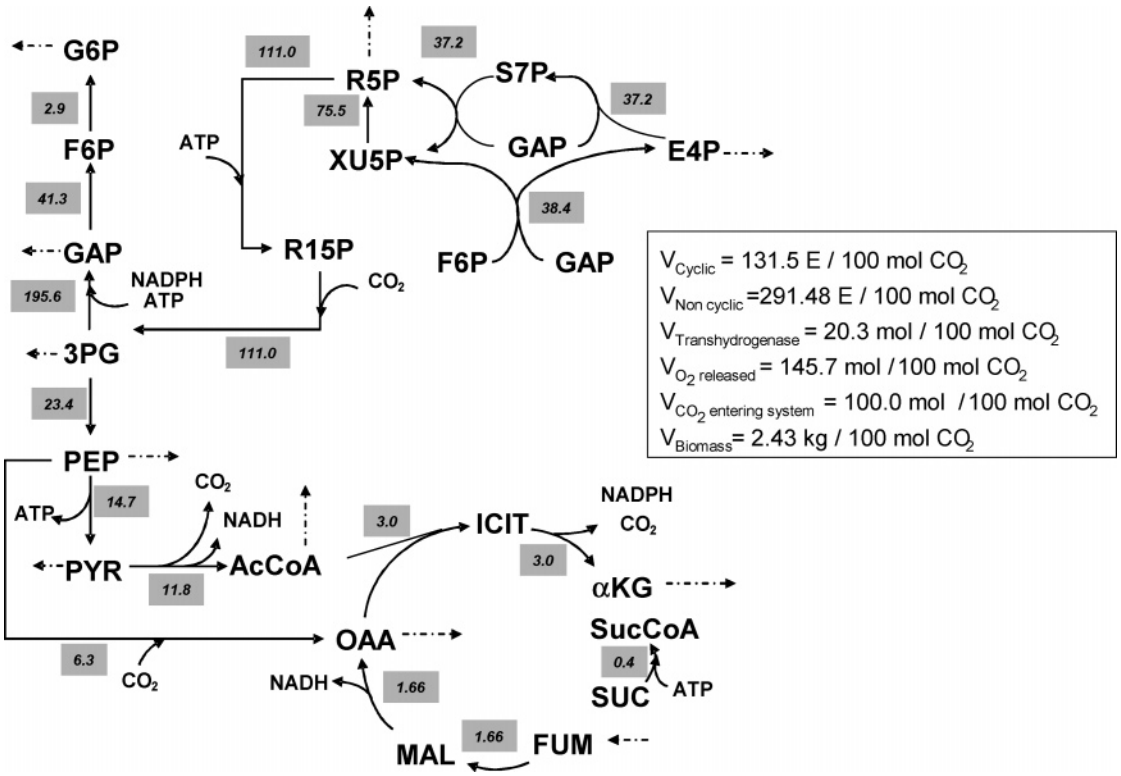

Figure 2. Autotrophic flux map. Net flux values (mol/100 mol CO_2 assimilated) are highlighted in gray boxes. Linear pathways have been collapsed to obtain a compact representation of the network topology. The dashed arrows indicate flux related to biomass formation. 1 E = 1 mol photons.

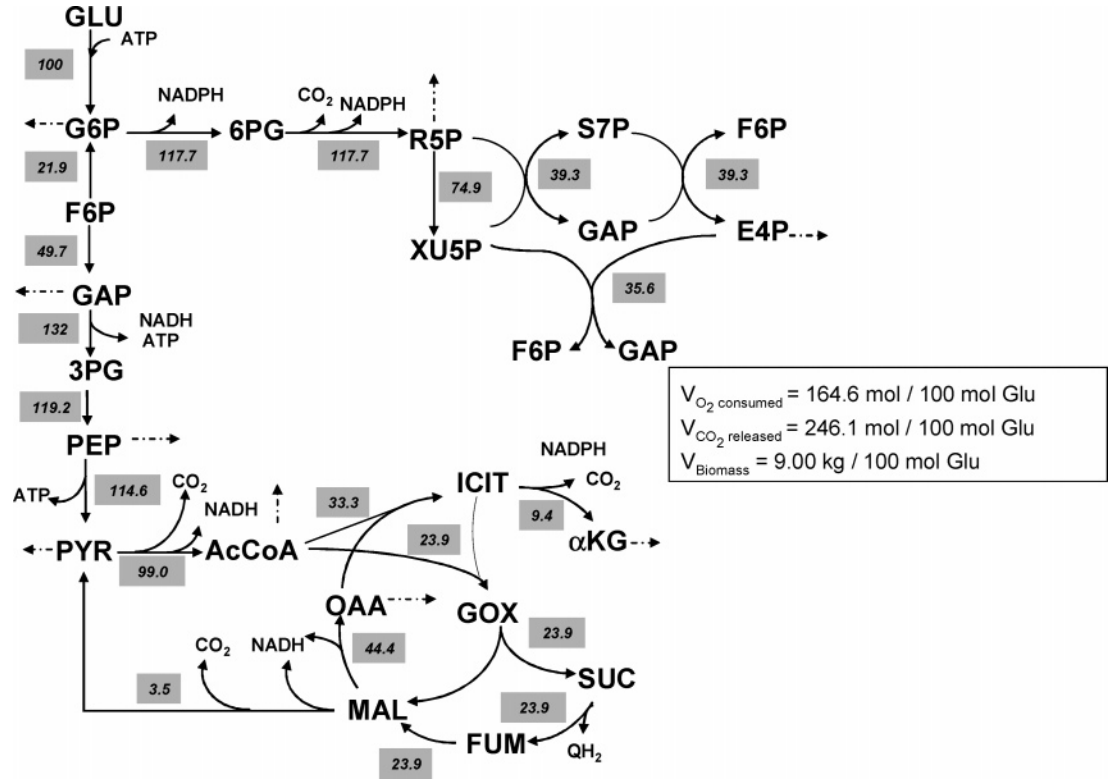

Figure 3. Heterotrophic flux map. Net flux values (mol/100 mol glucose uptake) are highlighted in gray boxes. Linear pathways have been collapsed to obtain a compact representation of the network topology. The dashed arrows indicate flux related to biomass formation.

tive pentose phosphate (Calvin cycle) and glycolytic pathways occurring simultaneously. The topology is interesting since a portion of but not the entire Calvin cycle is in operation. This type of network configuration was observed in developing embryos of rapeseed, which undergo mixotrophic growth (*33*).

Comparison of Yields. The autotrophic biomass yield is 24.3 g biomass/mol C contained in CO_2, whereas the

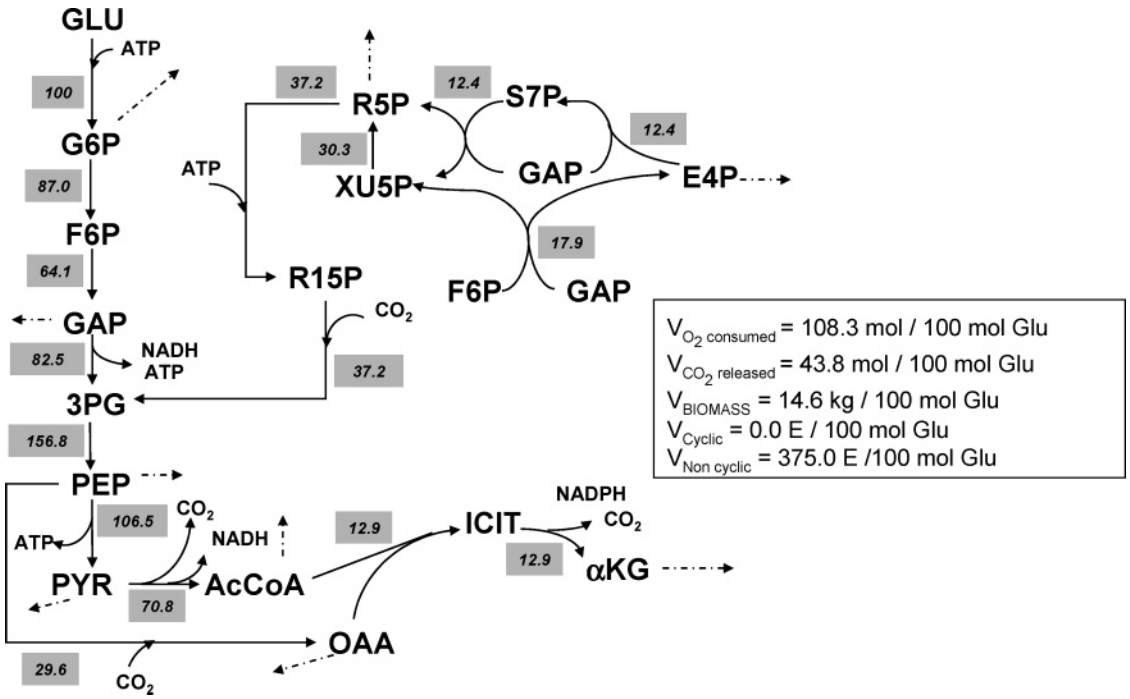

Figure 4. Mixotrophic flux map. Net flux values (mol/100 mol glucose uptake) are highlighted in gray boxes. Total light flux of 0.184 μE/m^2/s was provided to the system. Linear pathways have been collapsed to obtain a compact representation of the network topology. The dashed arrows indicate flux related to biomass formation. 1 E = 1 mol photons.

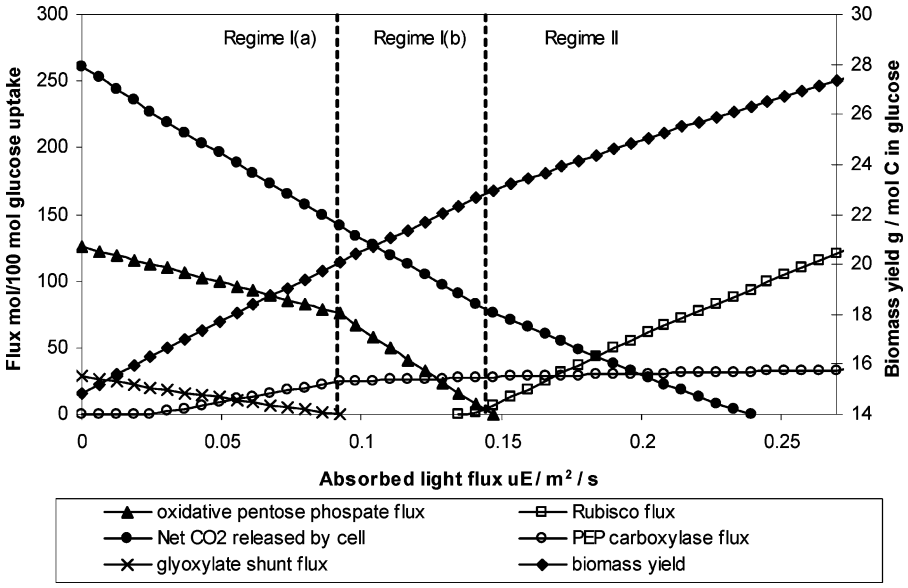

Figure 5. Variation of mixotrophic growth yields and fluxes as a function of light flux utilization.

Table 2. Comparison of Biomass Yields under Autotrophic, Heterotrophic, and Mixotrophic Conditions

growth condition	growth yield
autotrophic	24.3 g biomass/mol C in net CO_2 assimilated by cell
heterotrophic	15.0 g biomass/mol C entering cell via glucose
mixotrophic	Increases with increasing light flux from 14.9 g biomass/mol C entering via glucose to 26.3 g biomass/mol C entering via glucose (Figure 5)

heterotrophic biomass yield is 15.0 g biomass/mol C contained in glucose (Table 2). Clearly, in heterotrophic metabolism, 37% of the carbon in glucose is diverted toward producing energy (ATP) and is lost as carbon dioxide through the TCA cycle and oxidative pentose phosphate pathway (Figure 3), thereby resulting in a lower biomass yield.

For mixotrophic metabolism, the yield of biomass (g biomass/mol C in glucose) increased as the amount of light energy provided increased. This occurs in distinct regimes, as shown in Figure 5. In regime I(a), as the available light flux increases, the biomass yield increases linearly from the heterotrophic yield (g biomass/mol C in glucose) due to a decrease of CO_2 lost through the oxidative pentose phosphate flux and increase of CO_2 fixation by PEP carboxylase. The available light flux is utilized via the noncyclic ETC to produce both NADPH and ATP. The ability to derive NADPH from light also leads to a steady decrease in the oxidative pentose phosphate flux (Figure 5). The flux through the glyoxylate shunt drops linearly to zero. As the amount of

available light and hence NADPH increases, in regime I(b), the flux through the oxidative pentose phosphate pathway decreases rapidly to zero. The rate of C fixation flux through PEP carboxylase correspondingly increases at a slower rate than in regime I(a). Interestingly, the slope of biomass yield line remains the same in regimes I(a) and I(b). In the next regime (II), as sufficient light energy becomes available, CO_2 fixation occurs through the Calvin cycle. It can be seen that the increase in biomass yield per unit light energy provided is less in regime II since the Calvin cycle has a high energetic and reducing equivalent cost to fix each CO_2 (3 ATP, 2 NADPH per CO_2 fixed to 3PG).

Starting with the purely heterotrophic biomass yield, the mixotrophic yield increases until it equals the autotrophic yield. This point corresponds to incorporation of all of the glucose carbons into biomass through refixation of lost CO_2 using light flux. Any further increase in light flux leads to a constant increase in biomass yield (on a glucose basis), as is shown in Figure 5. The hetero- and autotrophic yield values in Figure 5 are slightly different from those obtained in the purely hetero- and autotrophic cases, since a mixotrophic biomass composition was used in the above series of simulations. It is to be expected, however, that the biomass composition changes as the trophic conditions are altered. We therefore checked validity of the above analysis by calculating the curve in Figure 5 with the heterotrophic and autotrophic biomass compositions. We observed similar qualitative trends for all these cases.

Batch mixotrophic growth of *Synechocystis* has been experimentally characterized under different light fluxes and different feed glucose concentrations (*34*). Due to the limited data in the literature, only qualitative comparisons between the reported experiments and simulations are possible. Experimentally it was found that when the system is provided with 1.5 g/L glucose, the mixotrophic biomass yield (g biomass/g glucose) increases with increasing light flux and subsequently saturates (*34*). Simulation results also show an increasing trend (Figure 5), with saturation type behavior seen at a light flux of approximately 0.85 $\mu E/m^2/s$.

Role of Glyoxylate Shunt. The glyoxylate shunt is predicted to be active under optimal heterotrophic growth conditions (Figure 3) and also under some mixotrophic conditions (Figure 5). This is consistent with the data obtained from ^{13}C labeling patterns observed experimentally under mixo- and heterotrophic conditions for *Synechocystis* (*15*). Although the glyoxylate shunt is not active in the photoautotrophic simulation (Figure 2), we expect non-zero flux through it as it is required to produce succinyl CoA as a cofactor required for growth. Since stoichiometric modeling assumes that there is already a sufficient pool of cofactors available under steady state conditions, it only predicts the routes of cofactor regeneration. Thus, our model predicts that succinyl CoA is regenerated via succinyl CoA synthetase from succinate (which is a byproduct of biomass formation) and ATP but does not predict the route of synthesis of the initial succinate pool itself. These three cases also indicate a dual role for the glyoxylate shunt in order to achieve optimal growth. The first is to produce succinyl CoA as described above to meet cofactor requirements, while the second is a is to provide the succinate which can be converted into fumarate, simultaneously reducing a quinone pool associated with the respiratory electron transport chain, as seen under heterotrophic conditions and some cases of mixotrophic growth.

Role of Transhydrogenase and Cofactor Balances. The autotrophic flux map for wild-type *Synechocystis* shows a transhydrogenase flux of 20.3 mol/100 mol C assimilated. To evaluate the role of the transhydrogenase, a mutant was simulated and found to be infeasible under zero respiration conditions. The role of transhydrogenase in this flux map was initially hypothesized to be either to produce NADPH or to regenerate NAD^+. If simultaneous respiration was permitted in silico, an equivalent flux of 20.3 mol/100 mol C was obtained for the respiratory regeneration of NAD^+. *Synechocystis* has both the respiratory and photosynthetic electron transport carriers in shared membranes (*35*), and it is plausible that transhydrogenase circumvents the necessity to simultaneously run the photosynthetic and respiratory electron transport chains, which inherently run in opposite directions. Additionally, there is evidence of negligible respiration under photoautotrophic conditions (*36*). Characterizing a transhydrogenase mutant would therefore be of interest to test this hypothesis. Since fluxes through the transhydrogenase are very sensitive to cofactor balances, the hypothesis must be treated with caution. We therefore propose to develop a more extensive model of electron transport in cyanobacteria that can take into account thylakoid membranes with common photosynthetic and respiratory electron carriers as well as cytoplasmic membranes with only respiratory electron carriers that have been observed experimentally in *Synechocystis* (*37*).

Role of Cyclic and Noncyclic Photophosphorylation. The relative contribution of cyclic and noncyclic photophosphorylation toward biochemical ATP production from photons is an important parameter in the characterization of autotrophic metabolism. Most experimental studies report the PSI to PSII ratio under different physiological conditions. These are sometimes qualitatively correlated to cyclic and noncyclic electron transport activity (*38*, *39*). However, quantitative correlation of the PSI/PSII ratio to the relative contribution of the two electron flow schemes toward ATP formation is complicated by the fact that some components, including PSI itself, are common to both ETCs. Our photoautotrophic simulations suggest that the optimum ratio of cyclic to noncyclic electron transport flux is 0.225 (normalized per electron flow through the ETCs), with the biosynthetic NADPH demand determining the contribution of noncyclic electron transport, and cyclic electron transport producing the remaining required ATP. On the basis of studies in *Arabidopsis thaliana*, Munekage et al. have shown cyclic electron transport to be essential for efficient photosynthesis and hypothesized that the noncyclic electron transport chain cannot produce the correct ATP/NADPH ratio without the aid of cyclic electron transport (*40*).

Evaluation of Enzyme Deletions or Additions. A reconstructed metabolic network model is a valuable tool to assess the metabolic capabilities of the organism with different genetic backgrounds. We selected a few specific enzyme targets from central metabolism and used our model to determine if they were necessary for growth of *Synechocystis*. The results were compared with reported mutants from the *Synechocystis* database (*14*). Table 3 summarizes the mutations that were evaluated. The GAP1 gene product is an NAD^+-dependent GAP dehydrogenase that converts GAP into PDG, which is then further converted into 3PG. The GAP2 gene codes for an NADPH-dependent GAP dehydrogenase that runs primarily in the opposite direction (*41*). We found that GAP2 knockouts cannot grow on CO_2 but can grow optimally

Table 3. Effect of Gene Deletions or Heterologous Gene Additions on Biomass Yield under Different Growth Conditions

knockout/addition (A)	reaction	change in biomass yield/quanta light	
		heterotrophic	autotrophic
malic enzyme	MAL + NAD^+ → PYR + CO_2 + NADH	inviable	0%
GAP1	GAP + NAD^+ → PDG + NADH	inviable	0%
GAP2	PDG + NADPH → GAP + $NADP^+$	0%	inviable
αKG dehydrogenase (A)	αKG + $NADP^+$ + COA → SUCCOA + CO_2 + NADPH	0.85%	0%
fumarate reductase (A)	FUM + QH_2 → SUC + Q	0%	0%

under heterotrophic conditions. GAP1 knockouts were able to grow optimally under autotrophic conditions but were inviable under heterotrophic conditions. These results are consistent with experimentally observed phenotype of GAP1 and GAP2 mutants (*41*).

The malic enzyme that converts malate into pyruvate and CO_2 was found to be essential for heterotrophic growth of *Synechocystis* but not for autotrophic growth. Although no mutants have been reported in the database, ^{13}C labeling studies on *Synechocystis* have shown the malic enzyme to be operational in heterotrophic growth on glucose (*23*). Contrary to the simulated results, the use of in vivo transposon mutagenesis of the malic enzyme demonstrated reduced photoautotrophic growth (*42*). The role of malic enzyme in photoautotrophic growth may therefore be some function other than stoichiometric demand, such as involvement in carbon concentration mechanisms (*23*).

To evaluate the metabolic capabilities of *Synechocystis*, which has an incomplete TCA cycle, simulations were performed with the addition of αkg dehydrogenase and fumarate reductase to the reaction network (see Table 3). Interestingly, no change in the autotrophic biomass flux map or increase in biomass yield was observed. Under heterotrophic conditions, however, the biomass flux increased by ca. 0.9%. We conclude that the absence of a complete TCA cycle does not significantly limit the growth yield of *Synechocystis*. Thus, we ruled out these enzymes as potential metabolic engineering targets for improved biomass yields.

Existence of Multiple Optimum Topologies. The feasible region of the linear programming problem can potentially contain multiple optimum solutions. Of these, the existence of alternative optimum topologies is particularly important, since different topologies represent different routes or pathways to obtain the same optimum objective value. We searched the solution space for the existence of multiple optimum topologies for the autotrophic and heterotrophic cases, using the method of Lee et al. (*43*). We also investigated the existence of multiple topologies in the mixotrophic case presented in Figure 4. No alternative optimal topologies could be identified in any of the cases. Although the autotrophic flux topology shown in Figure 2 may seem intuitive, we demonstrate that, given the reconstructed model, there are no other routes that result in equivalent optimum flux distributions.

Conclusions

A stoichiometric model of *Synechocystis* sp. PCC 6803 was reconstructed from genomic sequence and biochemical literature, including equations for cyclic and noncyclic photophosphorylation. Flux balance analysis coupled with linear programming was applied to photoautotrophic metabolism, leading to predictions on metabolic flux topologies under various physiological conditions. The metabolic roles of various network components such as the glyoxylate shunt, transhydrogenase, and cyclic and noncyclic photophosphorylation were analyzed within the limitations of steady-state stoichiometric models. Both cyclic and noncyclic electron transport were found necessary for optimal photoautotrophic growth. *Synechocystis* did not have multiple optimal flux topologies under autotrophic growth conditions. The model reconstruction also enabled the evaluation of various gene knockouts and additions with respect to optimal growth yield. The lack of a complete TCA cycle in *Synechocystis* did not affect biomass yield significantly.

Although the current model captures the global interactions of the conversion of light to chemical energy and central metabolism, the model can be improved. For example, a more detailed model of electron transport chain organization in the thylakoid and cytoplasmic membranes, which captures the interactions between components of the respiratory and photosynthetic electron transport chains, should be added. Inclusion of the efficiencies of light transmission, harvesting, and photochemical energy transduction is necessary for model validation. These improvements would lead to increased redox flexibility and therefore the presence of multiple optimum topologies will need to be reinvestigated. The model can be extended to explicitly include the metabolic reactions leading to the formation of various biomass components and storage compounds.

Notation

2PG	2-phosphoglycerate
3PG	3-phosphoglycerate
6PG	6-phosphogluconate
Ac	acetate
AcCoA	acetyl CoA
ADP	adenosine diphosphate
αKG	α-ketoglutarate
AMP	adenosine monophosphate
ATP	adenosine triphosphate
CoA	coenzyme A
E4P	erythrose 4-phosphate
ETC	electron transport chain
F6P	fructose 6-phosphate
FUM	fumarate
G6P	glucose 6-phosphate
GAP	glyceraldehyde 3-phosphate
GOX	glyoxylate
MAL	malate
NAD^+	nitcotinamide adenine dinucleotide (oxidized)
NADH	nitcotinamide adenine dinucleotide (reduced)
$NADP^+$	nitcotinamide adenine dinucleotide phosphate (oxidized)
NADPH	nitcotinamide adenine dinucleotide phosphate (reduced)
OAA	oxaloacetate
PDG	1,3-bisphosphoglycerate
PEP	phosphoenol pyruvate
PMF	proton motive force

PSI	photosystem I
PSII	photosystem II
PYR	pyruvate
Q	quinone (oxidized)
QH_2	quinone (reduced)
R15P	ribulose 1,5-diphosphate
R5P	ribose 5-phosphate
S7P	sedoheptulose 7-phosphate
SUC	succinate
SUCCoA	succinyl CoA
TCA	tricarboxylic acid cycle
X5P	xylulose 5-phosphate

Acknowledgment

The authors would like to thank Mr. Shuo-Huan Hsu for his technical assistance with linear programming. This project was funded by the e-Enterprise center, Discovery Park, Purdue University and the NSF CAREER award to J.A.M. (BES-0348458).

Supporting Information Available: Reactions of the stoichiometric model of *Synechocystis* sp. PCC6803 and for the formation of amino acids, nucleotides and other biomass components. This material is available free of charge via the Internet at http://pubs.acs.org.

References and Notes

(1) Bro, C.; Regenberg, B.; Forster, J.; Nielsen, J. Metabolic engineering in *Saccharomyces cerevisiae* through the use of a reconstructed genome-scale metabolic network leads to improved ethanol production. *Yeast* **2003**, *20*, S284−S284.

(2) Fernie, A. R.; Geigenberger, P.; Stitt, M. Flux an important, but neglected, component of functional genomics. *Curr. Opin. Plant Biol.* **2005**, *8*, 174−182.

(3) Morgan, J. A.; Rhodes, D. Mathematical modeling of plant metabolic pathways. *Metab. Eng*. **2002**, *4* (1), 80−89.

(4) von Caemmerer, S. *Biochemical Models of Photosynthesis*; Commonwealth Scientific and Industrial Research Organization Publications: llingwood, Victoria, Australia, 2000.

(5) Reed, J. L.; Palsson, B. O. Thirteen years of building constraint-based in silico models of *Escherichia coli*. *J. Bacteriol.* **2003**, *185*, 2692−2699.

(6) Varma, A.; Palsson, B. O. Metabolic capabilities of *Escherichia coli*. 1. Synthesis of biosynthetic precursors and cofactors. *J. Theor. Biol.* **1993**, *165*, 477−502.

(7) Edwards, J. S.; Palsson, B. O. Systems properties of the *Haemophilus influenzae* Rd metabolic genotype. *J. Biol. Chem.* **1999**, *274*, 17410−17416.

(8) Schilling, C. H.; Covert, M. W.; Famili, I.; Church, G. M.; Edwards, J. S.; Palsson, B. O. Genome-scale metabolic model of *Helicobacter pylori* 26695. *J. Bacteriol.* **2002**, *184*, 4582−4593.

(9) David, H.; Akesson, M.; Nielsen, J. Reconstruction of the central carbon metabolism of *Aspergillus niger*. *Eur. J. Biochem.* **2003**, *270*, 4243−4253.

(10) Famili, I.; Forster, J.; Nielsen, J.; Palsson, B. O. *Saccharomyces cerevisiae* phenotypes can be predicted by using constraint-based analysis of a genome-scale reconstructed metabolic network. *Proc. Natl. Acad. Sci. U.S.A.* **2003**, *100*, 13134−13139.

(11) Yang, C.; Hua, Q.; Shimizu, K. Energetics and carbon metabolism during growth of microalgal cells under photoautotrophic, mixotrophic and cyclic light-autotrophic/dark-heterotrophic conditions. *Biochem. Eng. J*. **2000**, *6*, 87−102.

(12) Burgard, A. P.; Pharkya, P.; Maranas, C. D. OptKnock: A bilevel programming framework for identifying gene knockout strategies for microbial strain optimization. *Biotechnol. Bioeng.* **2003**, *84*, 647−657.

(13) Kaneko, T.; Sato, S.; Kotani, H.; Tanaka, A.; Asamizu, E.; Nakamura, Y.; Miyajima, N.; Hirosawa, M.; Sugiura, M.; Sasamoto, S.; Kimura, T.; Hosouchi, T.; Matsuno, A.; Muraki, A.; Nakazaki, N.; Naruo, K.; Okumura, S.; Shimpo, S.; Takeuchi, C.; Wada, T.; Watanabe, A.; Yamada, M.; Yasuda, M.; Tabata, S. Sequence analysis of the genome of the unicellular Cyanobacterium *Synechocystis* sp. strain PCC6803. II. Sequence determination of the entire genome and assignment of potential protein-coding regions. *DNA Res.* **1996**, *3*, 109−136.

(14) Nakamura, Y.; Kaneko, T.; Hirosawa, M.; Miyajima, N.; Tabata, S. CyanoBase, a WWW database containing the complete nucleotide sequence of the genome of *Synechocystis* sp. strain PCC6803. *Nucleic Acids Res.* **1998**, *26*, 63−67.

(15) Yang, C.; Hua, Q.; Shimizu, K. Quantitative analysis of intracellular metabolic fluxes using GC-MS and two-dimensional NMR spectroscopy. *J. Biosci. Bioeng.* **2002**, *93*, 78−87.

(16) Voordouw, G.; Vandervies, S. M.; Themmen, A. P. N. Why are 2 different types of pyridine-nucleotide transhydrogenase found in living organisms. *Eur. J. Biochem.* **1983**, *131*, 527−533.

(17) Stal, L. J.; Moezelaar, R. Fermentation in cyanobacteria. *FEMS Microbiol. Rev.* **1997**, *21*, 179−211.

(18) Malkin, R.; Niyogi, K. Photosynthesis. In *Biochemistry and Molecular Biology of Plants*; Buchanan, B., Gruissem, W., Jones, R., Eds.; American Society of Plant Physiologists: Rockville, MD, 2000; pp 568−628.

(19) Allen, J. F. Photosynthesis of ATP−Electrons, proton pumps, rotors, and poise. *Cell* **2000**, *110*, 273−276.

(20) Albertsson, P. A. A quantitative model of the domain structure of the photosynthetic membrane. *Trends Plant Sci.* **2001**, *6*, 349−358.

(21) Genty, B.; Briantais, J. M.; Baker, N. R. The relationship between the quantum yield of photosynthetic electron-transport and quenching of chlorophyll fluorescence. *Biochim. Biophys. Acta* **1989**, *990*, 87−92.

(22) Emlyn-Jones, D.; Ashby, M. K.; Mullineaux, C. W. A gene required for the regulation of photosynthetic light harvesting in the cyanobacterium *Synechocystis* 6803. *Mol. Microbiol.* **1999**, *33*, 1050−1058.

(23) Yang, C.; Hua, Q.; Shimizu, K. Metabolic flux analysis in *Synechocystis* using isotope distribution from ^{13}C-labeled glucose. *Metabol. Eng.* **2002**, *4*, 202−216.

(24) Metting, F. B.; Smith, J. L.; Amthor, J. S.; Izaurralde, R. C. Science needs and new technology for increasing soil carbon sequestration. *Clim. Change* **2001**, *51*, 11−34.

(25) Loferer-Krossbacher, M.; Klima, J.; Psenner, R. Determination of bacterial cell dry mass by transmission electron microscopy and densitometric image analysis. *Appl. Environ. Microbiol.* **1998**, *64*, 688−694.

(26) Lawerence, B. A.; Suarez, C.; DePina, A.; Click, E.; Kolodny, N. H.; Allen, M. M. Two internal pools of soluble polyphosphate in the cyanobacterium *Synechocystis* sp. strain PCC 6308: An in vivo P-31 NMR spectroscopic study. *Arch. Microbiol.* **1998**, *169*, 195−200.

(27) Pirt, S. J. Maintenance energy of bacteria in growing cultures. *Proc. R. Soc. London, Ser. B 163*, 224−231, 1965.

(28) Varma, A.; Palsson, B. O. Metabolic capabilities of *Escherichia coli*. 2. Optimal-growth patterns. *J. Theor. Biol.* **1993**, *165*, 503−522.

(29) Dubois, M.; Gilles, K. A.; Hamilton, J. K.; Rebers, P. A.; Smith, F. Colorimetric method for determination of sugars and related substances. *Anal. Chem.* **1956**, *28*, 350−356.

(30) Ishida, T.; Hasegawa, N.; Hayashi, N. R.; Peerapornpisal, Y.; Ishii, M.; Igarashi, Y.; Kodama, T. Growth characteristics and dense culture of a thermophilic cyanobacterium, *Chroococcidiopsis* sp. strain TS-821. *J. Ferment. Bioeng.* **1997**, *83*, 571−576.

(31) Neidhardt, F. C.; Ingraham, J. L.; Schaechter, M. *Physiology of the Bacterial Cell. A Molecular Approach*; Sinauer Associates, Inc.: Sunderland, MA, 1990.

(32) Buesa, R. J. Photosynthetic quotient of marine plants. *Photosynthetica* **1980**, *14* (3), 337−342.

(33) Schwender, J.; Goffman, F.; Ohlrogge, J. B.; Shachar-Hill, Y. Rubisco without the Calvin cycle improves the carbon efficiency of developing green seeds. *Nature* **2004**, *432*, 779−782.

(34) Wang, Y. H.; Li, Y. G.; Shi, D. J.; Shen, G. M.; Ru, B. G.; Zhang, S. L. Characteristics of mixotrophic growth of *Synechocystis* sp in an enclosed photobioreactor. *Biotechnol. Lett.* **2002**, *24*, 1593−1597.
(35) Appel, J.; Phunpruch, S.; Steinmuller, K.; Schulz, R. The bidirectional hydrogenase of *Synechocystis* sp PCC 6803 works as an electron valve during photosynthesis. *Arch. Microbiol.* **2000**, *173*, 333−338.
(36) Ryu, J. Y.; Suh, K. H.; Chung, Y. H.; Park, Y. M.; Chow, W. S.; Park, Y. I. NADPH dehydrogenase-mediated respiratory electron transport in thylakoid membranes of the cyanobacterium *Synechocystis* sp PCC 6803 is inactive in the light. *Mol. Cells* **2003**, *15*, 240−244.
(37) Berry, S.; Schneider, D.; Vermaas, W. F. J.; Rogner, M. Electron transport routes in whole cells of *Synechocystis* sp strain PCC 6803: The role of the cytochrome bd-type oxidase. *Biochemistry* **2002**, *41*, 3422−3429.
(38) Murakami, A.; Fujita, Y. Regulation of photosystem stoichiometry in the photosynthetic system of the cyanophyte *Synechocystis* pcc-6714 in response to light-intensity. *Plant Cell Physiol.* **1991**, *32*, 223−230.
(39) Satoh, A.; Kurano, N.; Senger, H.; Miyachi, S. Regulation of energy balance in photosystems in response to changes in CO_2 concentrations and light intensities during growth in extremely-high-CO_2-tolerant green microalgae. *Plant Cell Physiol.* **2002**, *43*, 440−451.
(40) Munekaga, Y.; Hashimoto, M.; Miyaka, C.; Tomizawa, K. I.; Endo, T.; Tasaka, M.; Shikanai, T. Cyclic electron flow around photosystem I is essential for photosynthesis. *Nature* **2004**, *429*, 579−582.
(41) Koksharova, O.; Schubert, M.; Shestakov, S.; Cerff, R. Genetic and biochemical evidence for distinct key functions of two highly divergent GAPDH genes in catabolic and anabolic carbon flow of the cyanobacterium *Synechocystis* sp. PCC 6803. *Plant Mol. Biol.* **1998**, *36*, 183−194.
(42) Zhang, S. L.; Laborde, S. M.; Frankel, L. K.; Bricker, T. A. Four novel genes required for optimal photoautotrophic growth of the cyanobacterium *Synechocystis* sp strain PCC 6803 identified by in vitro transposon mutagenesis. *J. Bacteriol.* **2004**, *186*, 875−879.
(43) Lee, S.; Palakornkule, C.; Domach, M. M.; Grossmann, I. E. Recursive MILP model for finding all the alternate optima in LP models for metabolic networks. *Comput. Chem. Eng.* **2000**, *24*, 711−716.

Accepted for publication September 25, 2005.

BP050246D